J. Comp. Physiol. 140, 59–68 (1980)

Journal of Comparative Physiology · A

Geometrical Optics of the *Notonecta* Eye: Adaptations to Optical Environment and Way of Life

Rudolf Schwind

Institut für Zoologie der Universität Regensburg, Universitätsstrasse 31, D-8400 Regensburg, Federal Republic of Germany

Accepted July 22, 1980

Summary. 1. Certain features of the optical geometry of the *Notonecta* dioptric apparatus were studied. The cornea consists of two homogeneous layers; in the distal layer the refractive index is high, and in the proximal layer it is low. The two are separated by a bell-shaped transition region. This aspherical zone has almost exactly the shape one would anticipate in a system corrected for spherical aberration (Fig. 10). The outer surfaces of the individual corneal lenses are only slightly convex; therefore there is little change in the position of the plane of focus in the eye when the animal leaves the water.

2. The ommatidia, perpendicular to the corneal surface in the central region, lie at progressively greater angles at positions further medial and lateral (Fig. 3); for this reason the whole compound eye has a broad visual field (Fig. 11) despite its slight curvature.

3. 75% of the optical axes of all the ommatidia are in the binocular visual space.

4. Observation of the displacement of the pseudopupil during rotation of the animal about a transverse axis reveals two zones of high acuity (Fig. 5). An animal resting below the water surface looks horizontally through the water with one of these zones. The other high-acuity zone is very small and lies $43° \pm 3°$ further ventral, so that it aims at the water surface just beyond the edge of the totally reflecting zone. With these ommatidia the animal can see the space just above the water surface.

5. In the ventral part of the eye the lattice of the optical axes is arranged in such a way that the vertical extent of a small object is always imaged in the same number of ommatidia regardless of distance, when the object is in the range 4.5 to 1.5 cm and 1 to 0 cm in front of the animal in the plane of the water surface. The range 1.5 to 1 cm is viewed by the high-acuity zone with which the animal scans the surface.

6. The extent to which the properties of movement-sensitive interneurons (Schwind, 1978) are based on the measured gradients in the optical lattice is discussed.

Introduction

Notonecta is a predatory aquatic insect that can also live in air. In its typical position it hangs just below the water surface, with its back down. In this situation its optical environment is subdivided into three zones: the totally reflecting water surface, the transparent water surface, and the underwater region.

In the work described here optical properties of the dioptric apparatus and features of the lattice of optical axes were examined. An attempt is made to document adaptations to the peculiarities of the animal's habits and habitat.

Materials and Methods

Both male and female *Notonecta glauca* were used for the experiments; no sex-specific differences in eye structure could be discerned.

1. Measurement of Focal-Point Position. The focal distance $S'F'$, between the innermost point on the corneal lens and the focal point in image space, was measured directly by a method like that of Vogt (1974). The focal length f in object space was determined from the size of the image of a slit aperture at a distance equivalent to infinity for the lens. The crystalline cells were replaced by water during this measurement. The error thus introduced was computed for the cornea as illustrated in Fig. 1b. It was always $< 5\%$ for both $S'F'$ and f. The directly measured data were multiplied by appropriate correction factors.

2. Determination of Index of Refraction. Sections had been cut with a Leitz freezing microtome. The refractive indices of single layers in the dioptric apparatus were determined with a Zeiss interference microscope equipped with a rotary compensator designed by Ehringhaus. This method was first applied to insect eyes by Seitz (1968). The quantity measured is the difference in path length travelled by two coherent light bundles, one of which passes

0340-7594/80/0140/0059/$02.00

through the object and the other through the adjacent embedding medium (water).

The difference in path length is given by (1) $G_0 = d \cdot (n_0 - n_m)$, where d is the thickness of section, n_0 the refractive index of the object, and n_m the refractive index of the medium (water). The difference in path length G_0 is proportional to the section thickness. For the proximal and the distal homogeneous layers a mean value for G_0 was obtained from sections examined in series (three series for each, each series comprising 10 5 µm thick sections). Errors associated with variation in section thickness thus averaged out. The refractive index is obtained by rearrangement of Eq. (1): (2) $n_0 = (G_0/d) + n_m$. The following checks were used to determine whether the 5 µm-setting of the microtome employed here did in fact produce a mean section thickness of 5 µm. 1) The microtome stage rose 200×5 µm = 1,000 µm after a series of 200 sections with the 5 µm-setting. 2) Sections of a short rectangular piece of methylmethacrylate of known refractive index proved to have an average thickness of 5 µm. Thickness was determined from formula (3): $d = G_0/(n_0 - n_m)$. Although there was considerable variation in thickness from section to section, this fact has little bearing on the determination of the mean for the series since no section was omitted.

Lines of equal refractive index in the inhomogeneous zone were drawn from photographs of single corneae with different compensator settings. For calculation of the refractive index of these isorefraction lines from the path differences, the value of d in Eq. (2) was not the thickness of section for which the microtome was set, but rather was determined from the path difference at the proximal homogeneous cornea layer and its previously determined refractive index.

3. Computation of Ray Paths. The computer program used to calculate the ray paths is based on a repeated application of Snellius' law of refraction for passage of rays through centered refractive spherical surfaces. The program was written for a Wang-600 table computer with attached printer.

The program for calculating F_2 in Fig. 10 was written in Basic. F_2 consists of 1,100 segments of circles. The position of their centers along the optical axis and their radius of curvature was determined iteratively so that the deviation of their focal points from that of a preset value was always $< 0.0001f$.

4. Density of the Optical Lattice. Notonecta individuals were mounted in the center of a goniometer rotatable about two axes. For later orientation, marks were made on the eyes with white lacquer. Shortly before the measurement the animal was killed with acetic ester and placed, with the goniometer, in a tank filled with water to a level such that the head was just submerged. The pseudopupil was observed by reflected light (Leitz microscope with an Ultrapak dark-field adapter; objective, Leitz UO 4/01) from above, through the water surface. The preparation was turned in steps of 10° and after each turn shifted so that the center of the pseudopupil was just below the intersection point of the cross-hairs in the ocular of the microscope. The pseudopupil region was photographed with the cross-hairs superimposed. The curves of Figs. 5 and 8 were obtained by averaging 6 and 10 such series of photographs, respectively.

Results

A. Properties of the Dioptric Apparatus

1. How Do the Focal Lengths in Image and Object Space Change with the Transition from Water to Air?

The dioptric apparatus of the eye of *Notonecta glauca* consists of the cornea and the crystalline cells, at the proximal end of which (in the light-adapted state) an open rhabdom begins. The eye is of the acone type (Grenacher, 1879), having four crystalline cells in place of a secreted cone. Because the crystalline cells are optically homogeneous, with a refractive index only slightly greater than that of water (see following section), the distance $S'F'$ between the innermost point on the cornea and the focal point, and the focal length f on the object side of the cornea, can be measured with the isolated cornea without severe error after the crystalline cells have been replaced by water. Measurements were done on cornea facets from a central part of the eye.

The distance $S'F'$ and the focal length f were found to be as follows for the cornea bounded by water:

$$S'F' = 68.9 \pm 0.9 \text{ µm}, \quad f = 72.1 \pm 1 \text{ µm};$$

and for the cornea bounded by air:

$$S'F' = 61.04 \pm 1 \text{ µm}, \quad f = 51.6 \pm 0.6 \text{ µm}.$$

It is evident that the internal focal length changes very little with the transition from water to air, becoming ca. 8 µm (about 11%) shorter. The change in object-space focal length is greater, about 28%. This means that the acceptance angle of the dioptric apparatus is enlarged by about 1/3.

2. How Are Rays Bent in the Dioptric Apparatus?

According to Bedau (1911), the cornea is composed of two layers (cf. Fig. 1), the distal layer of a harder consistency than the proximal.

In the interference microscope two layers are detectable, and each of these can be regarded as optically homogeneous. The distal layer has high refractive index ($n_0 = 1.543 \pm 0.008$), while that of the proximal layer is lower ($n_0 = 1.455 \pm 0.005$). Between the two optically homogeneous layers is a narrow zone within which there is a sharp gradient in refractive index between the two values (cf. Fig. 1).

The refractive index of the crystalline cells, adjacent to the inner surface of the lens, was found to be $n_0 = 1.349 \pm 0.005$.

The outer surface of the cornea is only slightly convex. This fact explains the slight difference in focal-point position for contact with air and with water. The proximal refractive surface of the cornea is spherical to first approximation; the surfaces with the same refractive indices in the transition layer are not spherical, but bell-shaped.

In Fig. 1 b refractive indices and shapes of refracting surfaces (or lines of equal refractive index in the

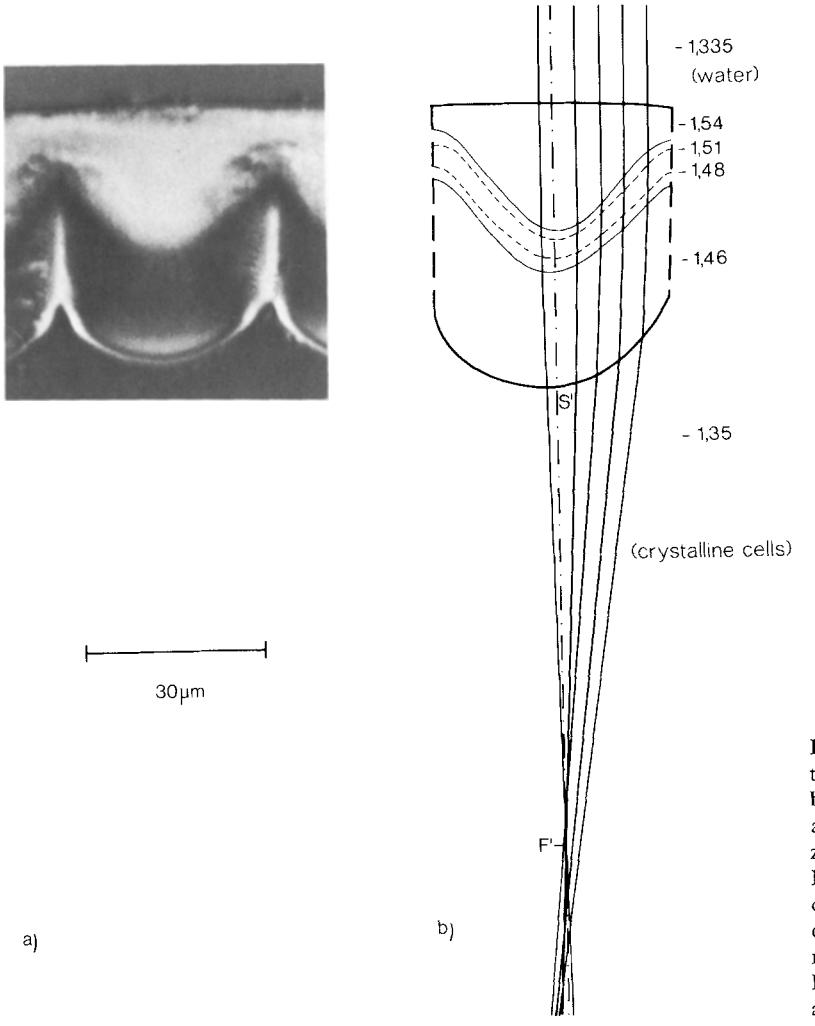

Fig. 1. a Interference micrograph of a section through a corneal facet. Section thickness, 3.5 µm. **b** Refractive indices and ray paths. Between two approximately homogeneous layers is a bell-shaped zone within which refractive index changes rapidly. Dot-and-dash line: optical axis. The ray to the left of the optical axis was computed; it intersects the optical axis at F'. The further off-axis rays on the right were drawn by geometric construction. Peripheral and central rays intersect the optical axis within a narrow region

transition zone) are indicated for the cornea shown in Fig. 1 a. The ray drawn just to the left of the optical axis in Fig. 1 b was calculated with a computer program for determining ray paths through spherical refracting surfaces. The ray intersects the optical axis at a distance of 73.9 µm from the innermost point on the cornea.

This calculation employs the radii of the circular arcs that most closely approximate the refracting surfaces or the isorefraction lines. (Five circles were used for the transition zone between the two homogeneous layers. The computation was simplified by taking the regions between the best-approximation arcs as optically homogeneous.)

The rays on the right, further from the optical axis, were constructed by taking tangents at the points of intersection of the ray with the isorefraction lines and with the refracting surfaces. The computed near-axis ray and the constructed rays further off-axis intersect the optical axis within a relatively small region.

Measurement of the intact cornea confirmed that the corneal lenses have very little spherical aberration. The diameter of the photographed image of a light source ($\lambda_{max} = 546$ nm) that can be taken as a point for practical purposes is $d = 2.04 \pm 0.07$ µm – no larger than the theoretical value for the diameter of the central diffraction disk

$$d' = 2 \cdot 1.22 \frac{\lambda \cdot f'}{D \cdot n}.$$

For an image-space focal length of 90 µm and a lens diameter of 40 µm, $d' = 2.24$ µm. (For method see Vogt, 1974.)

3. Slanted Doptric Apparatus

In horizontal sections through the eye one finds ommatidia of radially symmetrical structure only in the middle region, between the median and lateral periph-

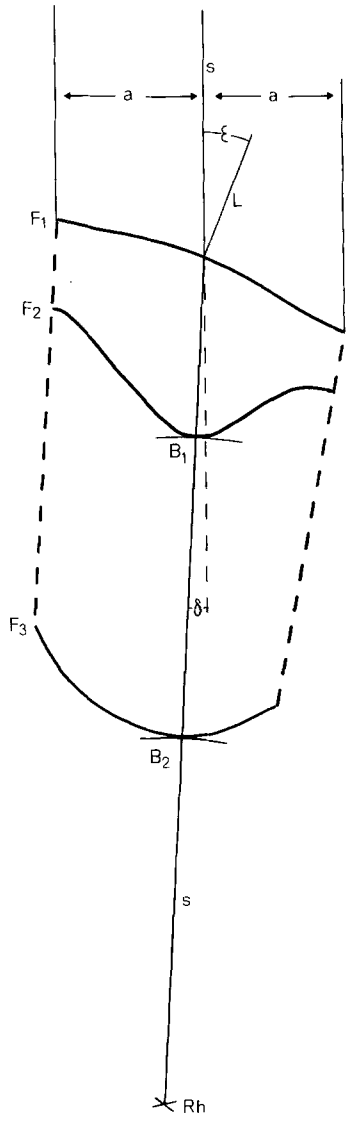

Fig. 2. A dioptric apparatus in the peripheral zone of the eye; its long axis is at an angle to the corneal surface. Only the distal limit of the optically inhomogeneous zone in the middle is shown. The ray s strikes the surface of the cornea in the middle of the facet, and reaches the middle of the rhabdom at the point Rh. The part of this line in object space corresponds to the optical axis of the ommatidium. For further discussion see text

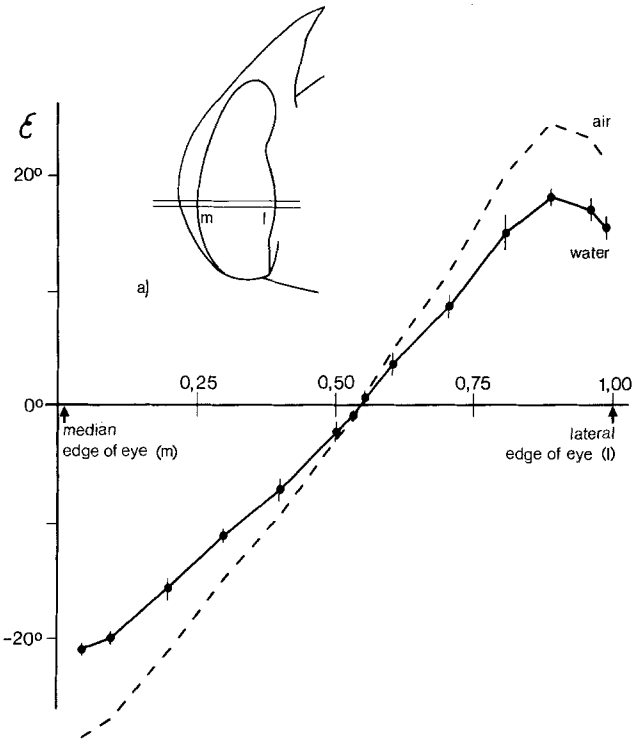

Fig. 3. Ordinate: the angle ε between the optical axes and a line perpendicular to the corneal surface (cf. Fig. 2). —: ε calculated for water; ---: ε calculated for air. Abscissa: position on eye surface. O: median edge of eye; 1: lateral edge of eye

eral zones. In these peripheral regions the dioptric apparatus is slanted. Figure 2 is a sketch of such a slanted ommatidium. The incident ray striking the cornea in the middle, between the two marginal rays, reaches the middle of the rhabdom (Rh). The part of the ray in object space corresponds to the optical axis (Exner, 1891). At the corneal surface this ray s is refracted by the angle δ. The remaining refractive surfaces of the cornea do not bend s; all the ommatidia examined had a dioptric arrangement such that s intersects these areas at the points of contact of arcs centered on the point Rh (B_1, B_2 in Fig. 2). s is thus perpendicular to F_2 and F_3 at the points of intersection.

ε is the angle between the optical axes and the line perpendicular to the surface of the cornea. In the diagram of Fig. 3, ε (as a measure of ommatidial slant) is plotted as a function of the position of the ommatidium in a horizontal plane of section (see Fig. 3 inset). Apart from the small region on the far right, the curves rise almost in a straight line. The ommatidia near the center of the eye, where $\varepsilon = 0$, would be symmetrical, and the further mediad or laterad an ommatidium is from this spot, the more slanted its orientation.

ε was measured in scale drawings of unstained methyl-methacrylate sections ($n=8$); in these drawings the optical axis of each ommatidium appearing in median longitudinal section was constructed. To avoid distortion, the methyl-methacrylate was not dissolved out of the sections.

B. Regional Differences in Density of the Optical Lattice

The shift of the pseudopupil during rotation of the animal within two orthogonal planes was measured. In many insect eyes the pseudopupil appears as a

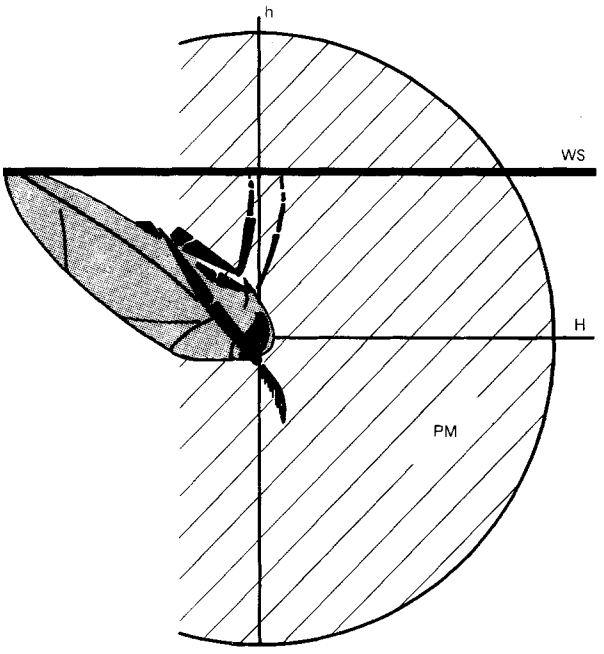

Fig. 4. Position of the paramedian plane (*PM*) and horizontal plane (*H*) for which $\Delta\phi$ is plotted in Figs. 5 and 6, respectively. *h* vertical axis; *WS* water surface

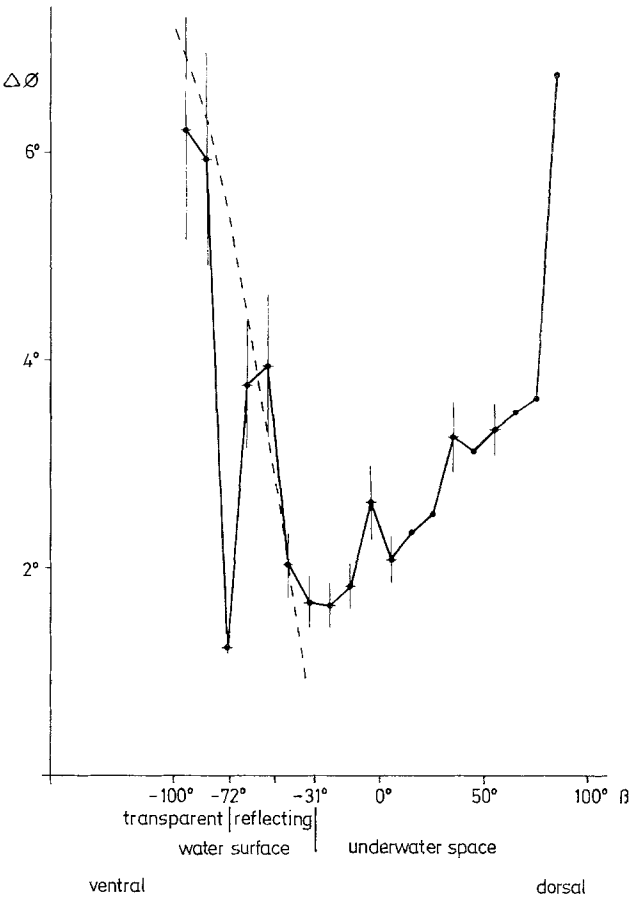

Fig. 5. Ordinate: the angle $\Delta\phi$ by which the animal must be turned about its transverse axis in order for the pseudopupil to move across the eye by one facet diameter. $\Delta\phi$ corresponds to the divergence angle between adjacent ommatidia, if the isopupil line lies parallel to a row of ommatidia. Abscissa: position of the optical axis in the dorsoventral plane. $\beta = 0°$ corresponds to the direction of the long axis of the body. $\beta = -31°$ corresponds to the horizontal, for an animal hanging under the water surface. There is a minimum in divergence angle in the vicinity of $\beta = -31°$, and another minimum at $-74° \pm 3°$, just beyond the boundary of the totally reflecting zone. Dashed curve: angle, with respect to the head of a bug hanging underwater, subtended by a partially submerged object of diameter equal to 0.07 the body length of *Notonecta*

dark zone at the place on the eye where the optical axes of the ommatidia are directed toward the observer (Exner, 1891). By observing its displacement when the eye is turned, one can obtain a better measure of divergence angle than by examining histological sections (Burkhardt et al., 1966; Seitz, 1968; Beersma et al., 1975; Horridge, 1978. Stavenga, 1979, describes the various pseudopupil phenomena).

To obtain the curve of Fig. 5, the animal was rotated about its transverse axis; the direction of observation was perpendicular to this axis. The optical axes of the ommatidia in the middle of the pseudopupil in each position lie in a paramedian plane in this case (PM in Fig. 4). In the diagram of Fig. 5 the abscissa indicates the angle β, in the paramedian plane, between the optical axes and the long axis of the body. On the ordinate is plotted the value $\Delta\phi = \Delta\alpha \cdot D/\Delta U$, where $\Delta\alpha$ is the angle by which the animal was turned, D is the mean diameter of the cornea facets in the region of the eye involved, and ΔU is the displacement of the pseudopupil during the rotation. $\Delta\phi$ corresponds to the angle through which the animal must be turned to move the pseudopupil a distance equivalent to the diameter of a facet. In the following $\Delta\phi$ will be referred to as the "divergence angle" for convenience, but note that it corresponds precisely to the divergence angle between adjacent ommatidia only when the line the pseudopupil follows during turning (the 'isopupil line'; Horridge, 1978) is parallel to a row of ommatidia. In the plane studied here this was not the case. Apart from a small region in the ventral part of the eye ($\beta < -80°$) where the corneal facets are rectangular, the isopupil line is as shown in Fig. 6.

The actual divergence angle between ommatidia placed with respect to one another like those marked with stars in Fig. 6 can be obtained from the curve by multiplying the values in the curve by $\sqrt{3}$. The smallest departures from the values given by the curve are to be expected for ommatidia in the y rows that are near the isopupillar line, because the y rows intersect the isopupillar line at the smallest angle (25°).

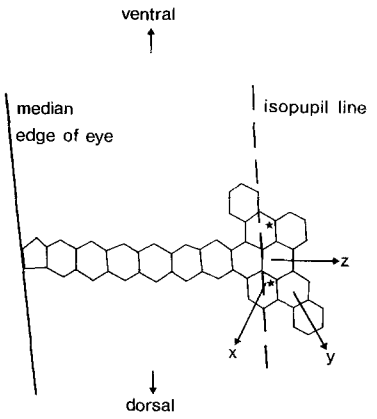

Fig. 6. Orientation of the isopupil line for the ommatidia with direction of view parallel to the dorsoventral plane. $\beta = -30°$ for the indicated z row

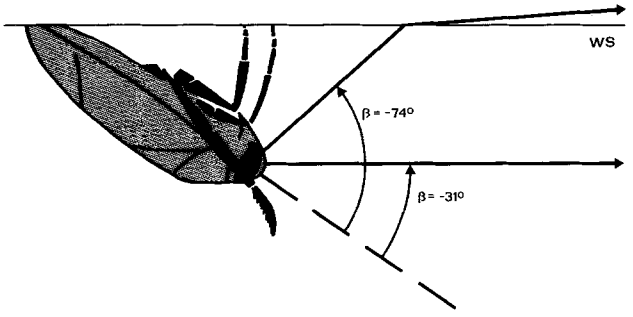

Fig. 7. There are two high-acuity zones, with optical axes diverging by more than 40°. When *Notonecta* is hanging below the water surface (*WS*) one of these looks underwater parallel to the surface, and the other looks just above the surface

The divergence angles in the vicinity of $\beta = -30°$ are verry small. $\beta = -31°$ corresponds to the position of the horizontal through the eye of an animal hanging below the water surface in resting position (Fig. 7). The divergence angles between ommatidia in more dorsal and more ventral regions increase progressively, except for a second, very narrow high-acuity zone at $\beta = -74° \pm 3°$. A line at this angle intersects the water surface just inside the boundary between the transparent and totally reflecting regions, which corresponds to $\beta = -72°$. When hanging below the surface the animal can scan the space just above the water with this zone of high resolution (Fig. 7), for rays entering the water at an angle near the limiting angle are bent sharply.

The dashed curve in Fig. 5 indicates the angle (ordinate) subtended by a spherical object seen by a *Notonecta* underwater, when the object is in front of the animal in the plane of the water surface. The abscissa now represents the position of the object in the median plane. The diameter of the object was chosen to be 0.07 times the body length of *Notonecta*,

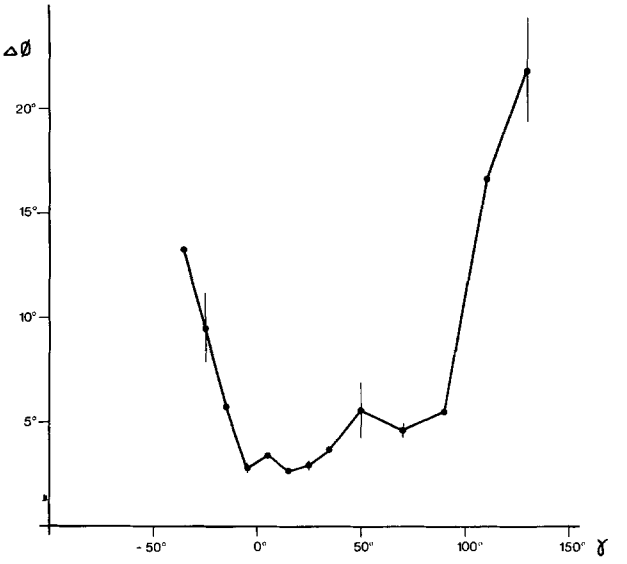

Fig. 8. $\Delta\phi$ for the horizontal plane (*H* in Fig. 4). γ: angle with respect to the median plane of the optical axes in the horizontal plane. Negative angles represent lines of view toward the contralateral side

so that the dashed curve coincides with the solid curve at $\beta = -44°$. Apart from the great disparity at $\beta = -74°$, the curve measured for $\Delta\phi$ follows the dashed curve in the range between $\beta = -40°$ to $\beta = -110°$.

The implication of this result is as follows. Except for the specialized, narrow zone with which *Notonecta* looks above the water surface, the vertical extent of a small object intersecting the water surface in the near region[1] ahead of *Notonecta* is always imaged by the same number of ommatidia, regardless of its distance from the animal. The vertical extent of a prey animal extending over 0.28 times the *Notonecta* body length in the median plane would be seen by 4 ommatidia.

Figure 8 shows $\Delta\phi$ for the horizontal plane (*H* in Fig. 4). The animal was turned about the vertical axis (*h*, Fig. 4) for this measurement. Note that the divergence angles are small for the ommatidia that aim forward ($\gamma = 0$), increasing very rapidly toward the midline (negative values of γ).

C. Binocular Visual Field

Figure 9 shows the extent of the binocular visual field. As in Fig. 5, β corresponds to the angle through which the animal is turned about the transverse axis. γ was measured along great circles perpendicular to

[1] Near region means a distance from 0 cm to 4.5 cm in front of the animal. At greater distances fewer ommatidia are stimulated. The narrow high-acuity zone, within which the abovementioned rule does not hold, is in the region between 1.5 and 1 cm

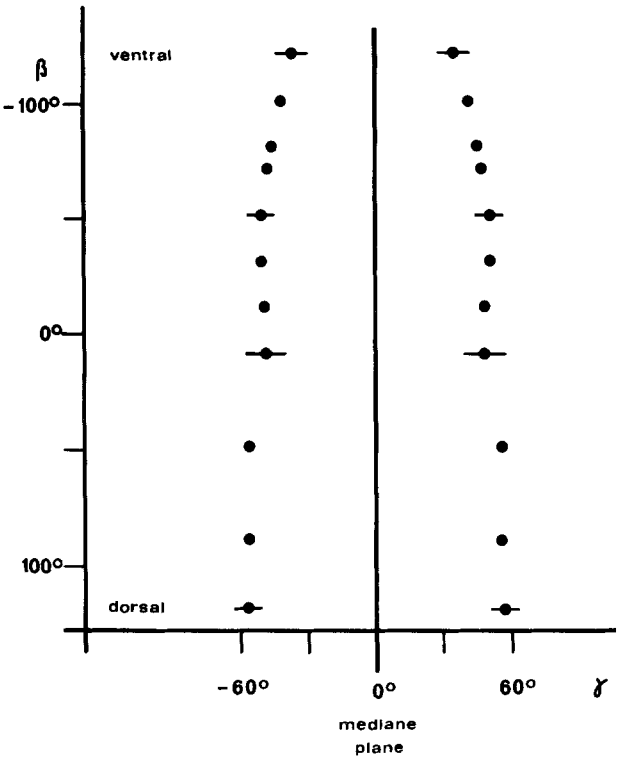

Fig. 9. Extent of the binocular visual field. β is the angle in the median plane with respect to the long axis of the body. γ was measured along great circles perpendicular to the median plane

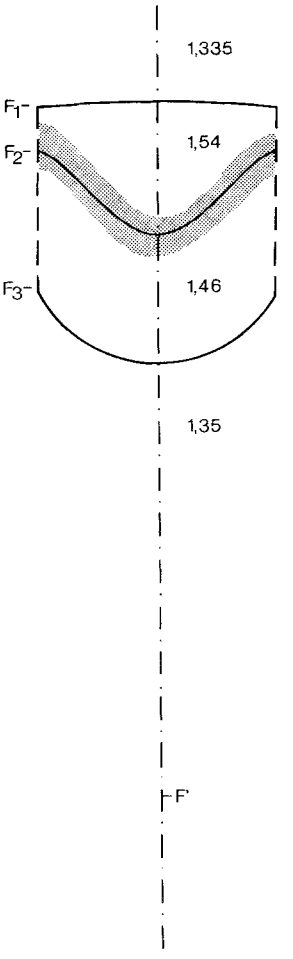

Fig. 10. Solid lines: lens system corrected for longitudinal aberration by means of calculated aspherical refractive surface F_2. Gray zone: aspherical refractive zone visible within the cornea shown in Fig. 1. See text for further explanation

the median plane. This form of representation of the binocular visual field is like that of Beersma et al. (1977)[2]. The boundaries of the binocular field measured with the pseudopupil method are in approximate agreement with the findings of Lüdtke (1935; 40° in the ventral part of the eye, 47° in the middle and 60° in the dorsal part). Photographs showing the line of pseudopupils at the boundary between the monocular and the binocular parts of one eye revealed that only 932 of 3,695 ommatidia were lateral to this line; the majority, ca. 75% of all the ommatidia, view areas within the binocular visual field.

Discussion

The distal surface of each corneal facet of *Notonecta* is only slightly convex. The development of nearly flat lens surfaces can be interpreted as an adaptation to the two different media, water and air. The corneal lenses of other water bugs also, as a rule, have little curvature. For example, all the water bugs examined by Bedau (1911) have almost flat corneal surfaces. The facets of most land bugs, by contrast, are distinctly convex. The advantage of nearly flat facets to the species living primarily in water is that the position of the focal point within the eye changes only slightly when the animal emerges from the water, and there is little change in the amount of light captured by the rhabdomeres.

Since the almost plane surface of the cornea contributes very little towards focusing light rays, there must be other refractive zones in the dioptric apparatus with especially small radii of curvature. Thus the radius of curvature near the apex of the refractive bell-shaped zone within the cornea is considerably smaller than the radius of the cornea; and since the isorefractive lines continue out to the margin of the cornea, this zone cannot be other than aspherical.

Furthermore, the aspherical zone has almost exactly the shape one would anticipate in a system corrected for spherical aberration (Fig. 10). The heavy line F_2 indicates a calculated refractive surface whose

[2] The angle γ corresponds to the angle ζ in the Fig. 1 of Beersma et al. (1977). In this figure no angle corresponding to β was plotted

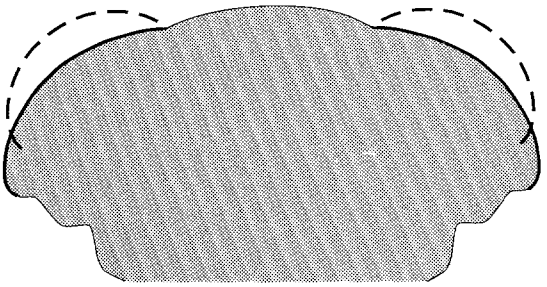

Fig. 11. Silhouette of the head (shaded); heavy lines denote the eye outline. Dashed lines indicate the shape the eyes would have to have if each dioptric apparatus were radially symmetrical

form permits all incident rays parallel to the optical axis to be focused at F'. The position of the apex of F_2 was defined prior to calculation and the spherical surfaces, F_1 and F_3, chosen to approximate the curvature of the outer and inner surfaces of the cornea. The indices of refraction correspond to those of water (1.335), the outer (1.54) and inner (1.46) homogeneous layers of the cornea and the crystalline cells (1.35). The position of F' corresponds to that of F' in Fig. 1. The shape of F_2 which was then calculated to correct for spherical aberration fits well into the bell-shaped zone of the cornea in Fig. 1. This zone was reproduced as the gray area in Fig. 10.

Since the diameter of the corneal lens is quite small, the advantages which accrue from correcting for spherical aberration are not large. On the other hand an uncorrected homogeneous lens of the same dimensions and with a higher refractive index so as to yield the same focal length as the cornea would have a wave front aberration of $A \approx 1$ at $\lambda = 546$ nm. With a spatial frequency corresponding to a wave length double the interommatidial angle ($\Delta\phi = 2°$) in the acute zone and for $\lambda = 546$ nm, the value of the frequency-response curve is 28% higher for the corrected system than it is for the uncorrected lens. For the calculations, which were based on the curves in Born and Wolf (1965, p. 488), the receiving plane of the uncorrected lens was located at the optimal position between the focal points for paraxial and marginal incident rays.

A refracting bell-shaped surface can also be found inside the lenses of certain trilobites. It is thought that these lenses were well corrected for spherical aberration (Clarkson and Levi-Setti, 1975).

The ommatidia of *Notonecta* lie at progressively greater angles to the eye surface as the edge of the eye is approached (Fig. 3). Compound eyes with this arrangement have a broad visual field although they are only slightly rounded (Exner, 1891). Figure 11 illustrates this effect in *Notonecta*. Over the outline of the head two dashed lines are drawn in to show the form an eye with the measured divergence angles would have if it were composed entirely of radially symmetrical ommatidia. (The outline of these more spherical eyes was calculated from the directions of the optical axes constructed for the ommatidia in the plane of section shown in Fig. 3.)

One advantage its flat eyes could offer *Notonecta* is that the animal encounters less resistance while swimming. It is striking that the agile swimmers among the water bugs, like *Notonecta* and *Corixa*, have eyes that protrude only slightly from the head. The sluggish *Ranatra*, by contrast, has rounded eyes (although the surface of each facet is nearly flat).

In the transition from water to air the position of the focal plane on the image side changes only slightly, but the focal length in object space – and thus the acceptance angles of the retinulae – increase by about 1/3. However, the overlap among the visual fields of adjacent ommatidia does not change to the same extent; the visual field of the whole eye and the divergence angles also are increased in air as compared with water, because of the slanting of the more peripheral ommatidia. In the transverse direction across the *Notonecta* eye, the increase in divergence angle is 0.4° in the central part and 0.5° in the periphery. For the ommatidia that aim forward (at $\gamma = 0°$ in Fig. 8) the increase in divergence angle amounts to about 18%.

An expansion of visual field in the air due to greater slant of the peripheral ommatidia was found by Exner (1891) in the *Limulus* eye. Kirschfeld and Reichardt (1964) noted that the acceptance and divergence angles in the *Limulus* eye change in the same direction.

Lüdtke (1953) reported morphological data on the size of a pigment aperture in light- and dark-adapted eyes. From his results, and from the values of focal length in object space and of divergence angle, one can estimate the effects of adaptation on effective acceptance angle. The conclusion is that the effective acceptance angle of an ommatidium in a light-adapted eye is not appreciably larger than the divergence angle, but that during dark adaptation it increases to more than 6 or 7 times the divergence angle. Similar relations have been found in *Lethocerus* (Ioannides and Horridge, 1975).

Ioannides and Horridge (1975) also discuss neural superposition in Hemiptera. Comments on neuroanatomical prerequisites for neural superposition, and further references, have been published by Wohlburg-Buchholz (1979).

75% of the ommatidia in the eye view the binocular visual field. Frantsevich and Pichka (1976) found similarly large percentages in other insects, primarily those that hunt prey in a structured environment – for example, *Aeshna* larvae (76%) and *Cicindela hybri-*

da (54%). A table of binocular field size is given by Burkhardt et al. (1973).

Irregularities in the density of the optical lattice can be regarded as typical of the apposition eyes of insects (Friedrichs, 1931; del Portillo, 1936; Zänkert, 1939; Horridge, 1978). Zänkert (1939) described a narrow-angled central zone in the *Notonecta* eye, that merges with wide-angled ventral and dorsal zones. A review of other remarks in the literature on regional variation in the *Notonecta* eye has been published by Meyer (1972/73). In the present study, observation of the pseudopupil has revealed that there is a second narrow-angled zone apart from the central region. This small zone, with very narrow divergence angles, is located in the ventral part of the eye, in such a position that when the animal is resting under the water surface these ommatidia view the space just above the surface. It remains to be discovered whether this ventral high-acuity zone also plays a special role during flying or swimming in the open water.

The diameter of the facets does not change in inverse proportionality to the divergence angles. Thus the product of divergence angle and facet diameter, the eye parameter $D \cdot \Delta\phi$ (Snyder, 1977), varies greatly in different parts of the eye. Figure 12 shows this variation over the array of ommatidia with optical axes parallel to the median plane of the animal (dotted curve, facet diameter; solid curve, the eye parameter $D \cdot \Delta\phi$). Similar variations of the eye parameter in different parts of the eye have been found in other insects for example, *Locusta* and the mantodean *Orthodera* (Horridge, 1978; possible interpretations of this eye structure are also discussed here).

In *Notonecta* the corneal facets in the ventral part of the eye, from about $\beta = -70°$, are smaller than in the middle and dorsal parts (Fig. 12). Because of the very small divergence angles and the small ommatidial diameter at $-74°$, the eye parameter is smallest here – even smaller than in the middle eye region of small-angle ommatidia viewing horizontally, at $-30°$ (the difference between the parameter value at $-74°$ and the individual points in the curve near $-30°$ is significant at the level $P < 0.05$).

This feature can be regarded as an adaptation to the light-intensity distribution in the surroundings of the animal hanging underwater. The smallest theoretically possible value of $D \cdot \Delta\phi$ is lower, the brighter the surroundings (Snyder, 1977). To a *Notonecta* hanging beneath the water surface the ventral part of the visual field, beyond $-72°$, is brighter than the remainder of the field, for the water surface is transparent in this region.

It has been emphasized repeatedly that the regional differences in size of the divergence angle must

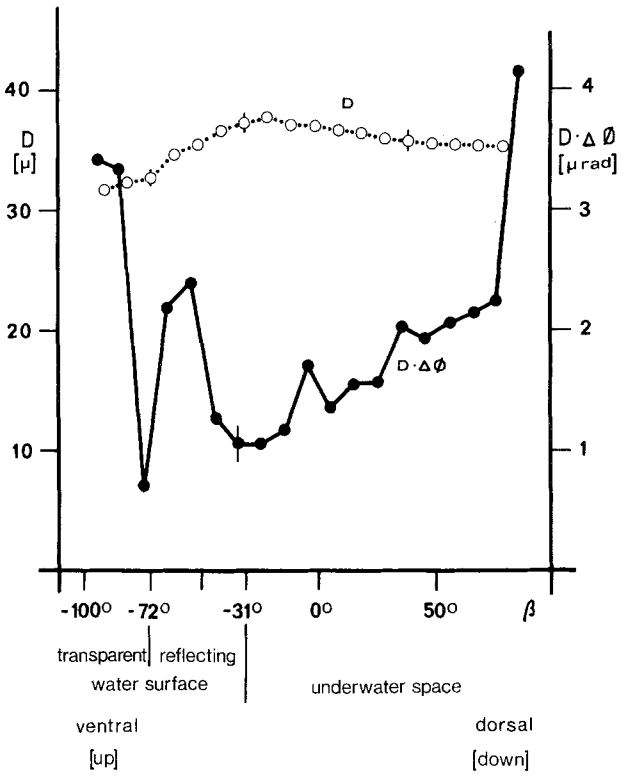

Fig. 12. Mean ommatidial diameter D and eye parameter $D \cdot \Delta\phi$, for the ommatidia aiming parallel to the median plane. β: angle between the optical axis and the direction of the long axis of the body

play an important role in visually guided behavior (Friedrichs, 1931; Del Portillo, 1936; Beersma et al., 1977; Horridge, 1978, who also gives further references). The findings in *Notonecta* support this notion, at least with regard to the structure of the ventral eye region. The zones of highest acuity aim in a horizontal direction when the animal is resting underwater, and the lattice of the optical axes in part of the ventral region is arranged in such a way that even at different distances the vertical extent, at least, of a prey animal moving on the water is always seen by the same number of ommatidia. The number of ommatidia involved in a visually guided approach does not therefore become unnecessarily large at close range. Moreover, it is conceivable that in this situation the neuronal network by which optimal prey size is recognized can be simpler than it would be with a uniform ommatidial raster.

There are certain movement-sensitive neurons in the visual pathway for which the position of maximal sensitivity in the receptive field changes as a function of the angle subtended by the stimulus object (Schwind, 1978). Small squares moved over a vertical arc elicited maximal responses when they crossed a position just above the horizontal, whereas larger

squares moving over the same arc were maximally effective at a further ventral position. One factor determining this neuronal property could be the increase in the vertical divergence angle toward the ventral edge of the eye. However, the excitation maximum was also shifted ventrad when the vertical angle subtended by the stimulus was kept constant and only its width was altered. No corresponding enlargement of the horizontal divergence angle in the ventral region was found. The results indicate that both gradients in the optical lattice and purely neuronal gradients contribute to the specific properties of the interneurons, and thus perhaps also to certain orientational abilities of the animal.

I thank the Deutsche Forschungsgemeinschaft for financial support, Prof. Burkhardt and Dr. de la Motte for critically reading the manuscript and for helpful discussions, Dr. Streng for writing the program for the calculation of F_2 in Fig. 10, Prof. Kirschfeld and Dr. Vogt for a discussion, Mrs Biederman-Thorson Ph. D. for translating the major part of the text, Dr. Loftus for the help to translate paragraphs 2 to 4 of the Discussion and Miss Humbs for technical assistance.

References

Bedau, K.: Das Facettenauge der Wasserwanzen. Z. Wiss. Zool. **97**, 417–456 (1911)

Beersma, D.G.M., Stavenga, D.G., Kuiper, J.W.: Organization and visual axes of compound eye of the fly *Musca domestica* L. and behavioural consequences. J. Comp. Physiol. **102**, 305–320 (1975)

Beersma, D.G.M., Stavenga, D.G., Kuiper, J.W.: Retinal lattice, visual field and binocularities in flies. J. Comp. Physiol. **119**, 207–220 (1977)

Born, M., Wolf, E.: Principles of Optics. 3. edn. London, New York: Pergamon Press 1965

Burkhardt, D., Darnhofer-Demar, B., Fischer, K.: Zum binokularen Entfernungssehen der Insekten. I. Die Struktur des Sehraumes von Synsekten. J. Comp. Physiol. **87**, 165–188 (1973)

Burkhardt, D., Motte, I. de la, Seitz, G.: Physiological optics of the compound eye of the blowfly. In: The functional organization of the compound eye. Bernhard C.G. (ed.), pp. 51–62. Oxford: Pergamon Press 1966

Clarkson, E.N.K., Levi-Setti, R.: Trilobite eyes and the optics of DesCartes and Huygens. Nature **254**, 663–667 (1975)

Del Portillo, J.: Beziehungen zwischen den Öffnungswinkeln der Ommatidien, Krümmung und Gestalt der Insektenaugen und ihrer funktionellen Aufgabe. Z. Vergl. Physiol. **23**, 100–145 (1936)

Exner, S.: Die Physiologie der facettirten Augen von Krebsen und Insecten. Leipzig, Wien: Deuticke 1891

Frantsevich, L., Pichka, V.E.: Dimensions of the binocular zone of the visual field of insects (in Russian). Zh. Evol. Biokhim. Fiziol. **12**, 461–465 (1976)

Friedrichs, H.F.: Beiträge zur Morphologie und Physiologie der Sehorgane der Cicindeliden (Col.) Z. Morphol. Ökol. Tiere **21**, 1–172 (1931)

Grenacher, H.: Untersuchungen über das Sehorgan der Arthropoden, insbesondere der Spinnen, Insekten und Crustaceen. Göttingen: Vandenhoeck und Ruprecht 1879

Horridge, G.A.: The separation of visual axes in apposition compound eyes. Philos. Trans. R. Soc. (London), Biol. **285**, 1–59 (1978)

Ioannides, A.C., Horridge, G.A.: The organization of visual fields in the hemipteran acone eye. Proc. R. Soc. (London), Biol. **190**, 373–391 (1975)

Kirschfeld, K., Reichardt, W.: Die Verarbeitung stationärer optischer Nachrichten im Komplexauge von *Limulus* (Ommatidien-Sehfeld und räumliche Verteilung der Inhibition). Kybernetik **2**, 43–61 (1964)

Lüdtke, H.: Die Funktion waagrecht liegender Augenteile des Rückenschwimmers und ihr ganzheitliches Verhalten nach Teillackierung. Z. Vergl. Physiol. **22**, 67–118 (1935)

Lüdtke, H.: Retinomotorik und Adaptationsvorgänge im Auge des Rückenschwimmers (*Notonecta glauca* L.). Z. Vergl. Physiol. **35**, 129–152 (1953)

Meyer, H.W.: Differenzierte Orientierungsleistung und räumliche Organisation des Insektenauges. Fortschr. Zool. **21**, 294–306 (1972/73)

Schwind, R.: Visual system of *Notonecta glauca:* A neuron sensitive to movement in the binocular visual field. J. Comp. Physiol. **123**, 315–328 (1978)

Seitz, G.: Der Strahlengang im Appositionsauge von *Calliphora erythrocephala* (Meig.). Z. Vergl. Physiol. **59**, 205–231 (1968)

Snyder, A.W.: Acuity of compound eyes: Physical limitations and design. J. Comp. Physiol. **116**, 161–207 (1977)

Stavenga, D.G.: Pseudopupils of compound eyes. In: Handbook of Sensory Physiology, Vol. VII/6A. Comparative physiology and evolution of vision in invertebrates. Autrum, H. (ed.), pp. 357–440. Berlin, Heidelberg, New York: Springer 1979

Vogt, K.: Optische Untersuchungen an der Cornea der Mehlmotte *Ephestia kühniella*. J. Comp. Physiol. **88**, 201–216 (1974)

Wohlburg-Buchholz, K.: The organization of the lamina ganglionaris of the hemipteran insects, *Notonecta glauca, Corixa punctata* and *Gerris lacustris*. Cell Tissue Res. **197**, 39–59 (1979)

Zänkert, A.: Vergleichend-morphologische und physiologisch-funktionelle Untersuchungen an Augen beutefangender Insekten. Sitzungsber. Ges. Naturforsch. Freunde Berlin **1–3**, 82–169 (1939)